Analysis and Design of a Novel Noncontacting Waveguide Backshort

Thomas M. Weller, *Student Member, IEEE,* Linda P. B. Katehi, *Senior Member, IEEE,* and William R. McGrath, *Member, IEEE*

***Abstract*—A new noncontacting waveguide backshort has recently been developed for millimeter- and submillimeter-wave frequencies. The design consists of a metal bar with rectangular holes cut into it, which is covered with a dielectric layer to form a snug fit with the broadwalls of a waveguide. It is mechanically rugged and can be readily fabricated for frequencies from 1–1000 GHz. This paper presents a technique for the theoretical characterization of the backshort, using an approach that combines the mode-matching method and a set of coupled space-domain integral equations. The convergence characteristics of the analysis are included, along with a set of general design guidelines.**

I. Introduction

WAVEGUIDES are currently used in a wide variety of applications covering a frequency range from 1 to over 600 GHz. In addition to the many commercial applications, NASA needs waveguide components for radiometers operating up to 1200 GHz for future space missions, and the Department of Defense is interested in submillimeter-wave communication systems for frequencies near 1000 GHz. One of the most frequent uses of the waveguide is as a variable length transmission line. These lines are used as tuning elements in more complex circuits, and may be formed by a movable short circuit, or backshort, in the waveguide. A conventional approach is to use a contracting backshort where a springy metallic material, such as beryllium copper, makes dc contact with the broadwalls of the waveguide. The contacting areas can degrade, however, due to wear from sliding friction. It is also extremely difficult to get uniform contact at frequencies above 300 GHz, where the waveguide dimensions become 0.5 $\times$ 0.25 mm for the 300–600 GHz band.

An alternative approach is the *noncontacting* backshort shown in Fig. 1. A thin dielectric layer (such as Mylar) prevents contact with the waveguide broadwalls and allows the backshort to slide smoothly. In order to produce an RF short, this backshort has a series of high- and low-impedance sections which are approximately $\lambda_g/4$ in length, where λ_g is the guide wavelength. The RF impedance of this design is given approximately by [1]

$$Z_{\mathrm{RF}} = \left(\frac{Z_{\mathrm{low}}}{Z_{\mathrm{high}}}\right)^{n} Z_{\mathrm{low}} \tag{1}$$

where Z_{low} is the impedance of the thick (low-impedance) sections, Z_{high} is the impedance of the thin (high-impedance) sections, and n is the number of sections. The thin sections, however, become difficult to fabricate for frequencies approaching 100 GHz, and may not even be feasible beyond 300 GHz. It would also be difficult to have the short slide snugly inside the waveguide at these high frequencies, as the thin sections would be very weak.

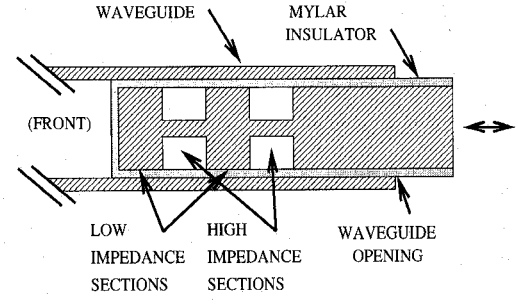

Fig. 1. Cross-sectional view of a conventional noncontacting backshort.

To circumvent these problems, a novel noncontacting backshort design has recently been developed [2]–[4] which is suitable for millimeter- and submillimeter-wave operation. It is a mechanically rugged design which can be readily fabricated for frequencies from 1–1000 GHz, and is thus a sound alternative to the miniaturization of conventional noncontacting shorts. The objectives of this paper are to discuss the new design and to outline an efficient method for its theoretical characterization that combines the mode-matching and integral equation techniques. The analysis has been used to confirm the experimentally observed performance and to determine general design guidelines for rectangular-hole backshorts, as presented in Section V-A. The results demonstrate that very good performance can be obtained over a broad bandwidth.

II. Novel Noncontacting Backshort

In order to obtain a large reflection of RF power, a noncontacting backshort must produce a series of properly phased smaller reflections of the incident wave. This is accomplished in the new design by either rectangular or circular holes, with the proper dimensions and spacing, cut into a metallic bar (see

Manuscript received May 6, 1993; revised September 12, 1994. This work was supported by the Innovative Science and Technology Office of the Ballistic Missile Defense Organization and the National Aeronautics and Space Administration, Office of Advanced Concepts and Technology.

T. M. Weller and L. P. B. Katehi are with the Radiation Laboratory, Department of Electrical Engineering and Computer Science, University of Michigan, Ann Arbor, MI 48109 USA.

W. R. McGrath is with the Center for Space Microelectronics Technology, Jet Propulsion Laboratory, California Institute of Technology, Pasadena, CA 91109 USA.

IEEE Log Number 9410322.

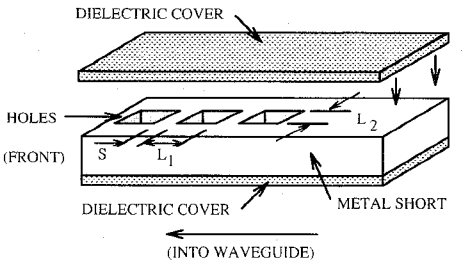

Fig. 2. The new noncontacting backshort design, shown with three rectangular holes. The size, shape, and spacing of these holes are important in determining the RF properties of the short. S is the spacing, L_1 is the length, and L_2 is the width of each hole. The front of the backshort is inserted into the waveguide opening.

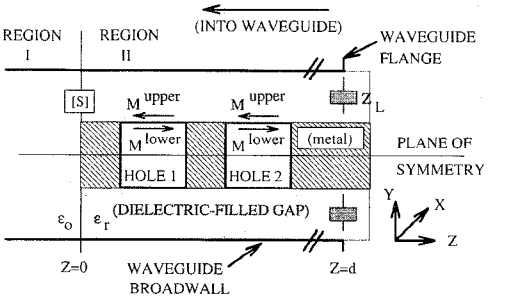

Fig. 3. Cross-sectional schematic diagram (not to scale) of a two-hole noncontacting backshort, inserted a distance d into the end of a waveguide. The waveguide broadwalls are on the top and bottom in the figure.

Fig. 2). This bar is sized to fit the waveguide cross section and slide smoothly with a dielectric insulator along the broadwalls and a small, air-filled gap on each side. The holes replace the thin-metal, high-impedance sections in the conventional design shown in Fig. 1, and actually provide a higher impedance since they extend completely through the bar. Furthermore, because the electromagnetic fields of the dominant mode are concentrated near the central axis of the waveguide and tend to zero at the sidewalls, the holes can be effective in producing large reflections of RF power, with the gaps along the sidewalls having a negligible effect. Finally, the new design is easy to fabricate and can be used at frequencies between 1 and 1000 GHz. For very high frequencies, above 300 GHz, the metallic bar is a piece of shim stock polished to the correct thickness. The holes can be formed by drilling, punching, or laser machining, or they can be etched using lithography techniques. Alternatively, silicon micromachining methods could be used for precision fabrication of the backshort. With regard to the dielectric layer, Mylar and kapton are commercially available with thicknesses down to 0.0085 mm, which is suitable for frequencies up to about 600 GHz. Oxide sputtering techniques or similar approaches could be used to apply even thinner dielectric layers.

III. Theoretical Formulation

Fig. 3 represents the cross-sectional view of a backshort with two holes, inserted a distance d into the end of a rectangular waveguide. The geometry is symmetric about the x–z plane, and the sides of the backshort are considered to be in contact with the sidewalls of the waveguide. Although sidewall gaps exist in the actual structure, the comparison between theoretical data and measured results indicates that the backshort can be accurately modeled using the assumption of dc contact on the sides. Misalignment of the backshort within the waveguide will result in the excitation of a coaxial-like TEM mode, as well as higher order TE or TM modes [15], which subsequently introduces dropouts in the return loss. This type of configuration would be difficult to model, however, and thus provisions for asymmetric positioning of the backshort have not been included in the analysis. Careful fabrication, furthermore, can minimize misalignment problems and mitigate these unwanted effects.

The formulation is based on the decomposition of the problem into two main components. In the first part, we compute the scattering matrix $[S]$ at $z = 0$, as depicted in Fig. 3. From $[S]$, the *incident* field in Region II, $\vec{H}^{\text{inc}}$, is determined given dominant-mode incidence from Region I. The second step is to solve for the reflection of $\vec{H}^{\text{inc}}$ due the presence of the holes. This is accomplished by closing the hole apertures with ficitious metal surfaces, upon which equivalent magnetic currents exist to satisfy field continuity requirements. Using the initial scattering at $z = 0$ and the additional radiation from the magnetic currents, one obtains the reflection coefficient for the dominant waveguide mode at the front of the backshort ($z = 0$). It is noted here that symmetry of the backshort about the x–z plane, which is the plane parallel to the waveguide broadwalls, has been utilized to reduce the number of unknowns. Furthermore, only rectangular holes (not round) have been considered in order to simplify the analysis. Neither of these points, however, is a necessary restriction in the formulation.

A. Scattering Matrix at $z = 0$ Reference Plane

As $[S]$ represents simply the scattering matrix for a waveguide discontinuity, the presence of the holes may be neglected, and thus becomes decoupled from the problem at hand. The well-documented mode-matching method, which has been used to solve a variety of waveguide problems [5]–[7] is applied to determine $[S]$. With this method, the fields at each side of the reference plane ($z = 0$) are expanded in infinite series of orthogonal mode pairs (e.g., TE-to-z and TM-to-z), and continuity of the tangential electric and magnetic fields is enforced to determine the scattered field amplitudes. This results in the following set of equations:

$$\sum_{n,m}^{\infty}(a_e^{\mathrm{I}}+b_e^{\mathrm{I}})\vec{\Phi}_e^{E,\mathrm{I}}+\sum_{n,m}^{\infty}(a_m^{\mathrm{I}}+b_m^{\mathrm{I}})\vec{\Phi}_m^{E,\mathrm{I}} = \sum_{n,m}^{\infty}(a_e^{\mathrm{II}}+b_e^{\mathrm{II}})\vec{\Phi}_e^{E,\mathrm{II}} + \sum_{n,m}^{\infty}(a_m^{\mathrm{II}}+b_m^{\mathrm{II}})\vec{\Phi}_m^{E,\mathrm{II}} \quad (2)$$

$$\sum_{n,m}^{\infty}(a_e^{\mathrm{I}}-b_e^{\mathrm{I}})\vec{\Phi}_e^{H,\mathrm{I}}+\sum_{n,m}^{\infty}(a_m^{\mathrm{I}}-b_m^{\mathrm{I}})\vec{\Phi}_m^{H,\mathrm{I}}$$
$$=\sum_{n,m}^{\infty}-(a_e^{\mathrm{II}}-b_e^{\mathrm{II}})\vec{\Phi}_e^{H,\mathrm{II}}$$
$$+\sum_{n,m}^{\infty}-(a_m^{\mathrm{II}}-b_m^{\mathrm{II}})\vec{\Phi}_m^{H,\mathrm{II}} \quad (3)$$

where (2) satisfies continuity of tangential $\vec{E}$ and (3) satisfies continuity of tangential $\vec{H}$. In the above, a and b represent the coefficients for waves traveling toward and away from the reference plane, respectively, and the vector functions $\vec{\Phi}$ contain the appropriate constants and x and y dependencies for the transverse components of the fields. The subscripts e and m are for TE-to-z and TM-to-z, while the superscripts denote the field type (electric or magnetic), as well as the region to which they pertain (to the left or right of the reference plane). At this point, inner products are formed using $\vec{\Phi}_e^{E,\mathrm{I}}$ and $\vec{\Phi}_m^{E,\mathrm{I}}$ with (2), and $\vec{\Phi}_e^{H,\mathrm{II}}$ and $\vec{\Phi}_m^{H,\mathrm{II}}$ with (3). Due to modal orthogonality, this step reduces (2) and (3) to a system of linear equations. This system is assembled into a matrix representation and, after inversion, the solution is expressed as

$$\{b\}^T=\{a\}^T[S] \quad (4)$$

where a and b are coefficient vectors and T denotes the transpose. Since the incident dominant TE_{10} mode has even symmetry about the $y = b/2$ plane, where b is the height of the large waveguide, it is necessary to analyze only the upper or lower half of the circuit.

The presence of a termination at $z = d$ (see Fig. 3) is accounted for by assigning

$$b^{\mathrm{I}}=a^{\mathrm{I}}S_{11}+a^{\mathrm{I}}S_{12}(I-\Gamma_L S_{22})^{-1}\Gamma_L S_{21} \quad (5)$$

where S_{ij} are the block submatrices of $[S]$, I is the identity matrix, and $[\Gamma_L]$ is a matrix which accounts for the reflection at $z = d$. As shown in the figure, we assume that the waveguide opening is terminated in a complex load Z_L for simplification. This approximation is necessary because the conditions outside the short are difficult to control experimentally and, likewise, difficult to characterize analytically. The matrix $[\Gamma_L]$ is thus a diagonal matrix of elements

$$(\Gamma_L)_{i,i}=\frac{Z_L-Z_g^i}{Z_L+Z_g^i}e^{-2\gamma_z^i d}=\rho_L^i e^{-2\gamma_z^i d}. \quad (6)$$

In (6), Z_g^i and γ_z^i are the wave impedance and complex propagation constant, respectively, for the ith TE/TM mode. Conductor and dielectric loss may be included in the factor γ_z^i. An approximate value of Z_L can be obtained by considering the impedance for a very thin aperture opening onto an infinite ground plane. In many test cases, the use of a normalized load impedance of $Z_L \approx (2.5 \pm 0.5)+j1$ yielded good agreement with the measured results. The predicted performance, however, is nearly independent of Z_L in the frequency bands where the backshort works well since most of the incident power is reflected and never reaches the end of the guide.

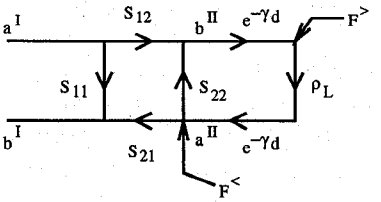

Fig. 4. Signal flow diagram for a backshort with holes.

B. Space Domain Integral Equation

The second step in the formulation is to apply the space domain integral equation technique to solve the boundary value problem at the aperture of each of the holes. The introduction of the equivalent magnetic currents $\vec{M}^{\mathrm{upper}}$ and $\vec{M}^{\mathrm{lower}}$ (see Fig. 3) allows the hole openings to be closed by a fictitious metallic surface, and thus transforms the backshort structure into a combination of a simple rectangular waveguide, which is the dielectric-filled gap region, and a series of isolated metallic cavities, which are the holes. These unknown magnetic currents radiate electromagnetic fields in the dielectric region, resulting in a modified form of (5). The new signal flow in Region II is illustrated by the diagram in Fig. 4. In this figure, a^{II} and b^{II} are the coefficients for the $+z$ and $-z$ traveling waves in the dielectric-filled gaps, respectively, and are given by

$$a^{\mathrm{II}}=\{a^{\mathrm{I}}S_{12}(I-\Gamma_L S_{22})^{-1}\Gamma_L\}$$
$$+\{(F^{>}\Gamma_L+F^{<})S_{22}(I-\Gamma_L S_{22})^{-1}\Gamma_L+F^{>}\Gamma_L\} \quad (7)$$

$$b^{\mathrm{II}}=a^{\mathrm{II}}S_{22}=\{a^{\mathrm{I}}S_{12}(I-\Gamma_L S_{22})^{-1}\Gamma_L S_{22}\}$$
$$+\{((F^{>}\Gamma_L+F^{<})S_{22}(I-\Gamma_L S_{22})^{-1}\Gamma_L$$
$$+F^{>}\Gamma_L)S_{22}\}. \quad (8)$$

The new expression for (5) is

$$b^{\mathrm{I}}=a^{\mathrm{I}}S_{11}+a^{\mathrm{I}}S_{12}(I-\Gamma_L S_{22})^{-1}\Gamma_L S_{21}$$
$$+\{(F^{>}\Gamma_L+F^{<})S_{22}(I-\Gamma_L S_{22})^{-1}\Gamma_L$$
$$+F^{>}\Gamma_L+F^{<}\}S_{21} \quad (9)$$

where the vector b^{I} contains the final dominant-mode reflection coefficient, S_{dm}, for the backshort. Note that the only unknown variables in these equations are $F^{<}$ and $F^{>}$, as the elements of the matrix $[S]$ and $[\Gamma_L]$ have previously been determined. These unknown components represent the coefficients of the fields due to the imposed equivalent magnetic currents, and their derivation is given below.

The solution for the unknown surface currents is uniquely determined by enforcing continuity of the total tangential fields across the hole apertures. Continuity of the tangential electric field is satisfied immediately by setting $\vec{M}^{\mathrm{upper}}=-\vec{M}^{\mathrm{lower}}=\vec{M}$. Assuming a backshort with N holes, continuity of the magnetic field at the kth hole leads to the following space domain integral equation (SDIE) in the unknown $\vec{M}$

$$-\hat{n}\times\vec{H}^{\mathrm{inc}}=\hat{n}\times\left\{\vec{H}^{\mathrm{scat}}+\sum_{n=1}^{N}\int\!\!\int_{S_n}ds'\,\overline{\overline{G}}_B\cdot\vec{M}_n\right.$$
$$\left.+\int\!\!\int_{S_k}ds'\,\overline{\overline{G}}_C\cdot\vec{M}_k\right\}. \quad (10)$$

As mentioned above, $\vec{H}^{\text{inc}}$ represents the known incident magnetic field, which results from scattering of the incoming wave at the waveguide step discontinuity (the reference plane). It is expressed in terms of TE and TM modes, the coefficients for which are given in the bracketed first terms of (7) and (8). $\overline{\overline{G}}_B$ and $\overline{\overline{G}}_C$ represent the dyadic Green's functions for magnetic currents in an *infinitely long* rectangular waveguide and a metallic cavity, respectively. Closed-form expressions for these functions can be derived using well-established boundary value formulations [8]. The use of $\overline{\overline{G}}_B$ in the dielectric-filled gap region, which does not directly satisfy the boundary conditions at $z = 0,\ d$ is possible by considering the fields to be a superposition of *primary* and *scattered* components. The primary components satisfy boundary conditions at the source, and radiate away from $\vec{M}$ assuming an infinite waveguide exists in either direction. These contributions are represented by the second term on the right-hand side of (10). The scattered components are also functions of $\vec{M}$, and are required to satisfy the boundary conditions away from the source at the discontinuity planes $z = 0,\ d$. These scattered fields, which are represented by $\vec{H}^{\text{scat}}$ in (10), are summations of TE and TM modes, and the coefficients for these modes are given in the second terms in (7) and (8).

The unknowns that have not yet been defined are $F^{<}$ and $F^{>}$. These are the coefficients for the fields radiated by the equivalent magnetic currents, which will be called the $\vec{M}$ fields. It is necessary to write these fields in terms of summations of TE and TM modes since the scattering matrix $[S]$ has been generated using a TE/TM representation, and $F^{<,>}$ and $[S]$ are directly related through (7)–(10). The general form for the fields radiated by $\vec{M}$ is given by

$$E^{<,>}_{z,x} = \sum_{n=1}^{N} \int\int_{S_n} ds' \left(\frac{-1}{\epsilon} \frac{\partial}{\partial y} G_B^{<,>} \right) (\hat{x} \cdot \vec{M}_n) = f^{<,>}_{z,x,E} e_z$$

$$H^{<,>}_{z,x} = \sum_{n=1}^{N} \int\int_{S_n} ds' \left(\frac{j}{\omega\epsilon\mu} \frac{\partial}{\partial z} \frac{\partial}{\partial x} G_B^{<,>} \right) (\hat{x} \cdot \vec{M}_n) = f^{<,>}_{z,x,H} h_z$$

$$E^{<,>}_{z,z} = 0 = f^{<,>}_{z,z,E} e_z$$

$$H^{<,>}_{z,z} = \sum_{n=1}^{N} \int\int_{S_n} ds' \left(\frac{j}{\omega\epsilon\mu} \left(k^2 + \frac{\partial}{\partial z} \frac{\partial}{\partial z} \right) G_B^{<,>} \right) \cdot (\hat{z} \cdot \vec{M}_n) = f^{<,>}_{z,z,H} h_z \tag{11}$$

where $<,>$ is used to differentiate between fields evaluated to the left or right of the source current locations, respectively. In the four $f^{<,>}$ variables, the first subscript denotes the field direction, the second the direction of the source current, and the third the type of field. The functions e_z and h_z contain the position dependence. By noting that TE and TM fields can be completely described in terms of the H_z and E_z components, respectively, it is observed that M_z will generate only TE modes, while M_x will generate both TE and TM modes. We now equate the form of $H^{<,>}_{z,\zeta}$ for each TE mode and $E^{<,>}_{z,x}$ for each TM mode, with the expressions that were used in the S-matrix formulation:

$$H^{<,>}_{z,x} = f^{<,>}_{z,x,H} h_z = c_1^{<,>} \alpha h_z$$

$$H^{<,>}_{z,z} = f^{<,>}_{z,z,H} h_z = c_2^{<,>} \alpha h_z$$

$$E^{<,>}_{z,x} = f^{<,>}_{z,x,E} e_z = c_3^{<,>} \beta e_z. \tag{12}$$

where α, β represent the leading modal constants used in the S-matrix formulation and c_1–c_3 are proportionality constants which depend on $\vec{M}_n$. The coefficients $F^{<,>}$ for the *equivalent* TE/TM form of the $\vec{M}$ fields may now be given as

$$F^{<,>}_{\text{TE}} = c_1^{<,>} + c_2^{<,>} \quad \text{(function of } M_x \text{ and } M_z\text{)}$$

$$F^{<,>}_{\text{TM}} = c_3^{<,>} \quad \text{(function of } M_x\text{)}. \tag{13}$$

The final step in the formulation is to solve the coupled set of integral equations which results from enforcing (10) over all N holes. This set is reduced to a system of linear equations by applying the method of moments (Galerkin's method) [9], an approach that has been proven to yield excellent results (see, for example, [10]–[12]). Using this procedure, the aperture of each hole is first divided into discrete subsections using a rectangular grid. The unknown currents are then expanded in terms of overlapping, piecewise sinusoidal basis functions of the form

$$\vec{M} = \sum_{ij} (\hat{x} M^x_{ij} f_j(x') \phi_i(z') + \hat{z} M^z_{ij} \phi_j(x') f_i(z'))$$

$$f_n(w') = \begin{cases} \dfrac{\sin[k(w' - w_{n-1})]}{\sin(kl_n)} & \text{if } w_{n-1} < w' < w_n \\ \dfrac{\sin[k(w_{n+1} - w')]}{\sin(kl_n)} & \text{if } w_n < w' < w_{n+1} \end{cases}$$

$$\phi_n(w') = \begin{cases} 1 & \text{if } w_{n-1} < w' < w_{n+1} \\ 0 & \text{else} \end{cases} \tag{14}$$

where M^x_{ij} and M^z_{ij} are constant coefficients, $(w = x,\ z)$, l_n is the length of the nth subsection in the x or z direction, and k is the wavenumber in the dielectric-filled waveguide region (used as a scaling parameter). This expansion is inserted into the integral equation, and inner products are formed using weighting functions which are identical to the basis functions. The coupled equations are thereby reduced to a matrix form which is solved for the unknown current coefficients $\vec{M}$. With $\vec{M}$ determined, all elements of (9) may be computed, and the solution is complete.

As a final note, minor modifications of the formulation are necessary in order to analyze a backshort with round holes. The primary difference is with $\overline{\overline{G}}_C$, which becomes the dyadic Green's function for a magnetic current inside a finite, cylindrical cavity. In addition, a staircase approximation to the hole apertures would be required.

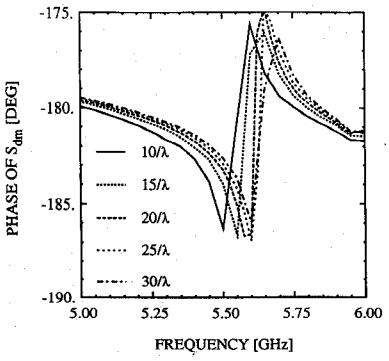

Fig. 5. The phase of the backshort reflection coefficient S_{dm} versus frequency for selected sampling rates. Maximum mode numbers are 800 for the dielectric region and 900 for the cavity region. The dielectric constant is 2.55.

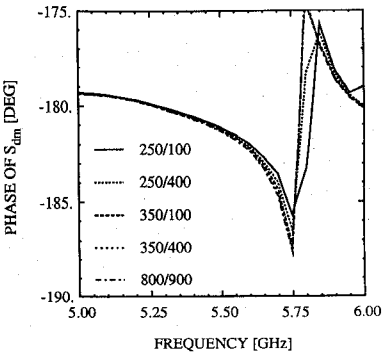

Fig. 6. The phase of the backshort reflection coefficient S_{dm} versus frequency for selected mode number pairs. The first number pertains to the dielectric region, while the second number pertains to the cavity region. The sampling frequency is $20/\lambda_g$. The dielectric constant is 2.4.

IV. Convergence

This section examines the convergence characteristics of the theoretical formulation. The stability of the numerical solution has been found to correspond directly with the resonant nature of the backshort, i.e., the solution converges very quickly in the frequency ranges where the backshort performs well (has a high reflection coefficient), but a much larger system is required in the frequency ranges where the backshort performance degrades (demonstrates dropouts in the reflection coefficient). The computation of the scattering matrix $[S]$, which uses the mode-matching method, requires only a few modes since the dimensions of the dielectric-filled gaps are very small. For the geometries investigated in this study, the solution converged with 15 TE and 6 TM modes included in each region. The majority of the computational effort involves the determination of the equivalent magnetic currents via the moment method. In terms of convergence, the parameters of interest are the sampling frequency and the maximum mode numbers, and these are examined below.

The cases studied will consider single-hole backshorts designed to operate from 4 to 6 GHz, which exhibit a dropout in the return loss of $\approx$ 2 dB around 5.6 GHz. The convergence behavior is not strongly affected by the number of backshort holes, such that the conclusions drawn for the single-hole case will also apply for multiple-hole backshorts. The phase of the reflection coefficient S_{dm} is used as the convergence criterion, although the magnitude would work equally well.

In the moment method solution, the sampling frequency refers to the size of the subsections used in the division of the hole aperture(s), and is measured in terms of the number of subsections per guide wavelength in the dielectric-filled regions. From Fig. 5, it is seen that a sampling frequency of $20/\lambda_g$ provides sufficient accuracy, and convergence of the phase minimum is obtained.[1] The improvements which could be gained by a higher sampling rate are outweighed by the additional computational effort that results from the increased size of the system.

The maximum mode numbers refer to the number of terms retained in the dyadic Green's function expansions, both in the dielectric-filled regions and in the cavities (i.e., inside the holes). The total number of terms is a product of the maximum $\hat{x}$ and $\hat{y}$ mode numbers, denoted as N_x and N_y, respectively, where the largest eigenvalues are $k_{x,\max} = N_x\pi/x_{\dim}$ and $k_{y,\max} = N_y\pi/y_{\dim}$. In the dielectric regions, the convergence has a very weak dependence on N_y because for most geometries $y_{\dim} \ll x_{\dim}$. An upper limit of $N_y = 10$ proved sufficient for all cases considered. The x–y dimensions of the cavities, however, are generally equivalent, and thus we take $N_x = N_y$ for the cavity functions. The results for the mode number tests, using a sampling frequency of $20/\lambda_g$, are given in Fig. 6. These curves indicate that a total of 350 modes are required in the dielectric region, while only 100 are needed inside the cavity.

[1] For a typical three-hole backshort, $20/\lambda_g$ sampling results in approximately 1000 unknowns.

V. Numerical Results

A. Design Guidelines

The theoretical analysis was used to develop a set of guidelines for the design of the noncontacting backshort with rectangular holes. Specifically, the goal was to optimize the performance of a one-hole backshort since multihole designs typically repeat the geometry of the first hole. It is important to note that the conclusions drawn here assume symmetric placement of the backshort within the waveguide, and are thus based on the best possible performance. In all cases examined, the waveguide size is 4.78 × 2.22 cm, and the backshort dimensions are 4.75 × 1.97 cm.

The design guidelines are geared towards two objectives, namely, maintaining the mechanical strength of the structure and obtaining an effective RF short over a broad bandwidth. The first objective is mostly dependent on the hole width and the backshort height, and with these fixed, the performance objective becomes a function of proper hole position and length. The mechanical aspects are very important for submillimeter-wave applications since the high-impedance sections of the backshort can become quite fragile. For this reason, it is desirable to minimize the hole width and at the same time provide a large RF reflection. The backshort height, on the other hand, should be maximized both for mechanical strength and for RF performance. The effectiveness of the short falls off quickly for sizes less than 85% of the waveguide height.

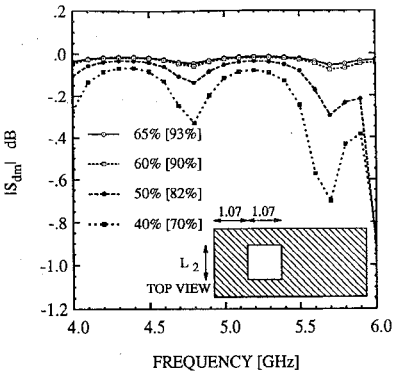

Fig. 7. Calculated reflection coefficient for a one-hole backshort for various hole sizes. The first number in the legend is the ratio of the hole width to the total waveguide width (×100%); the second number is the fractional power calculated from (15). The dielectric constant is 2.4 and the dimensions are in centimeters.

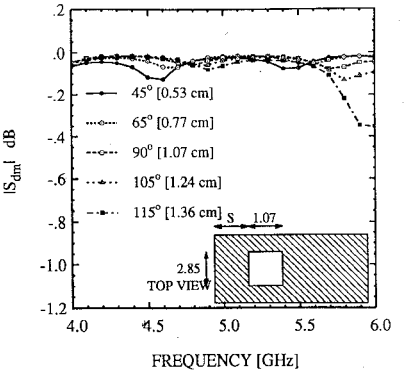

Fig. 8. Calculated reflection coefficient for a one-hole backshort for various hole spacings. The legend refers to the electrical length of the spacing S at the center frequency of 5 GHz. This is based on the wavelength of the TE_{10} mode in the dielectric filled gaps (16). The dielectric constant is 2.4 and the dimensions are in centimeters.

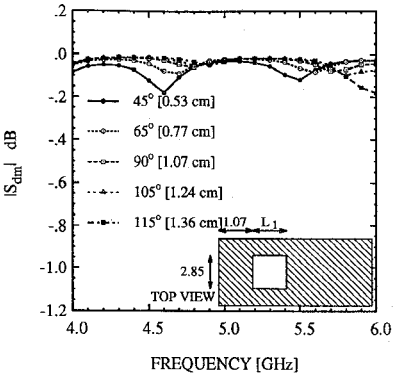

Fig. 9. Calculated reflection coefficient for a one-hole backshort for various hole lengths. The legend refers to the electrical length of the hole L_1 at the center frequency of 5 GHz. This is based on the wavelength of the TE_{10} mode in the dielectric filled gaps (16). The dielectric constant is 2.4 and the dimensions are in centimeters.

In the case of a one-hole design, there are three parts of the backshort which can potentially resonate and degrade the reflection: between the front of the backshort and the front edge of the hole, along the length of the hole, and between the back of the hole and the waveguide opening. The last two problems can be controlled to a significant degree by increasing the hole width, and thus a compromise is required between the mechanical strength and efficient reflection of power. To look at this quantitatively, consider the percentage of the power P_x which is carried by the dominant TE_{10} mode in a portion of the cross section of a waveguide. If this portion covers the height of the waveguide and $x\%$ of the width, then P_x is given by

$$P_x = x + \frac{\sin\left(\pi \frac{x}{100}\right)}{\pi} \text{ (percent)}. \tag{15}$$

Therefore, a hole which is only 60% as wide as the waveguide presents a discontinuity to 90% of the incident power. With the hole reflection in proper phase with the reflection at the front edge of the backshort, 60% width is sufficient to obtain a good balance between mechanical strength and RF performance. The degradation which results if the hole width is further decreased is illustrated by the curves in Fig. 7. Clearly, strong resonances develop when the hole becomes too narrow, and this problem will not be remedied by additional holes.

The remaining design specifications are the hole position and length. The hole position refers to the spacing between the front of the short and the first hole, and also between successive holes. In the ideal case of alternating low- and high-impedance sections, this distance should be $\lambda_{g,d}/4$ at the center frequency [1], where $\lambda_{g,d}$ is the guided wavelength of the TE_{10} mode in the dielectric filled gaps, and is given by

$$\lambda_{g,d} = \frac{\lambda_0}{\sqrt{\epsilon_r - \left(\frac{\lambda_0}{2A}\right)^2}}. \tag{16}$$

In this expression, λ_0 is the free-space wavelength, ϵ_r is the dielectric constant, and A is the width of the waveguide. From different test cases, it was found that electrical lengths between 65° and 105° at the center frequency provide very good performance over a 40% bandwidth (testing from 4 to 6 GHz). As shown in Fig. 8, dropouts in the return loss begin to appear as the spacing goes outside the stated limits. The optimum hole length, based on $\lambda_{g,d}$, falls within the same 65–105° range. In this specification, there may be a question as to why the length is based on the wavelength in the dielectric-filled gaps since the air-filled hole should alter the effective dielectric constant. The results in Fig. 9, however, show nearly the same characteristics as those seen in Fig. 8. This indicates that the ripples in the response are primarily caused by power which is trapped in the dielectric directly above and to the sides of the hole. In support of this, numerical tests have shown that the dropouts which result when the hole length approaches $\lambda_{g,d}/2$ are reduced as the hole width increases.

An additional design parameter is the dielectric constant of the material used for the insulator between the backshort and the waveguide broadwalls. As the electrical size of the backshort increases with increasing ϵ_r, more modes can propagate inside the dielectric-filled gaps and would be expected to degrade the performance. With the backshort positioned symmetrically within the waveguide, however, the higher order modes will not be strongly excited, and most of the power will still be carried by the dominant mode. To check this, the design guidelines stated above have been tested

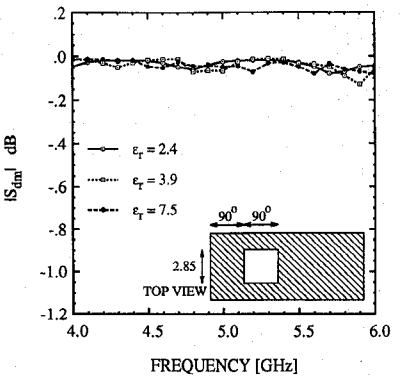

Fig. 10. Calculated reflection coefficient for a one-hole backshort using different dielectric constants. The hole width is 2.85 cm, and the spacing and length are 90° at 5 GHz, using the wavelength of the TE_{10} waveguide mode in the dielectric filled gaps (16).

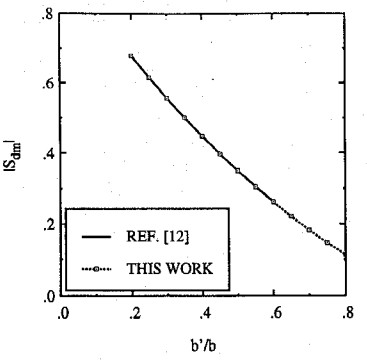

Fig. 11. Magnitude of the reflection coefficient S_{dm} from an asymmetric E-plane junction, where b is the height of the large waveguide and b' is the height of the small waveguide.

using dielectric constants of 2.4, 3.9, and 7.5, and the results are shown in Fig. 10. Except for differences in the small ripple across the band, the performance remains essentially unchanged.

B. Validation of Theory

The validation of the theoretical analysis of a backshort with holes was conducted by comparison with measured data. As a preliminary check, however, the calculated results for the scattering matrix $[S]$ at the waveguide discontinuity were compared with results found in [13], and the agreement was very good. In particular, results were compared for the reflection coefficient from asymmetric (i.e., single-step) E-phase and H-plane waveguide junctions. Fig. 11 shows the magnitude of the reflection coefficient $|S_{dm}|$ versus b'/b for an asymmetric E-plane junction, using $2b/\lambda_g = 0.4$, where λ_g is the guide wavelength, b is the height of the large waveguide, and b' is the height of the small waveguide.

In order to verify the design guidelines of Section V-A, a comparison between the performance of a backshort with and without holes is given in Figs. 12 and 13. For the 8–12 GHz frequency range, the waveguide dimensions are 2.286 × 1.016 cm and the backshort dimensions are 2.278 × 0.942 cm. Thin sheets of Mylar were used as the dielectric material, providing an effective dielectric constant of approximately 2.2.

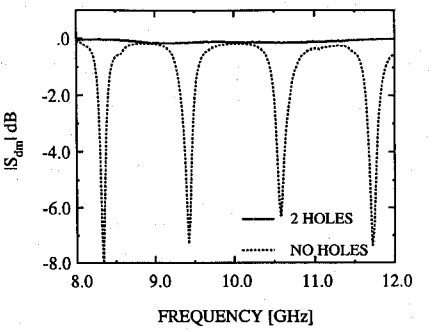

Fig. 12. Measured data showing the magnitude of the reflection coefficient for two backshorts. The solid line shows the performance for a design with two rectangular holes, sized according to the design guidelines. The dashed line indicates the performance of a backshort with no holes.

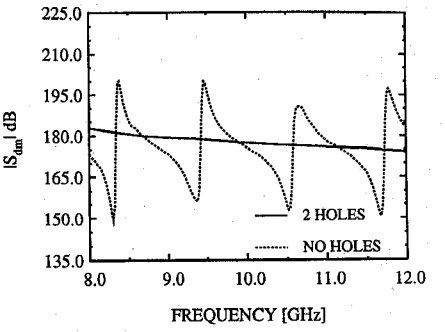

Fig. 13. Measured data showing the phase of the reflection coefficient for the same backshorts as in Fig. 12.

The two-hole backshort had holes which were 1.49 cm wide (65% of the waveguide width) with a length and spacing of 0.566 cm (90° at 10 GHz). The deep dropouts seen in Fig. 12 for the no-hole backshort occur at the resonant frequencies of the cavity formed in the dielectric-filled region, which is terminated by the front of the short and the waveguide opening. These dropouts are eliminated using the two-hole design, and the reflection coefficient is greater than −0.17 dB across the entire band. The phase performance for each backshort is shown in Fig. 13. The two-hole design has only approximately 8° of phase delay across the band, most of which is due to the Mylar sheets which are wrapped around the short, forming a thin dielectric layer on the front face.

VI. Conclusion

In summary, we have presented the analysis of a noncontacting waveguide backshort which consists of a metallic bar with holes cut into it. This new geometry combines high performance with design simplicity, and thus has the potential to be easily scaled for applications at high submillimeter-wave frequencies. Convergence studies on the moment method solution involved in the theory have shown that a sampling frequency of $20/\lambda_g$, with 350 modes in the waveguide regions and 100 modes in the cavity regions, provides sufficient accuracy. Furthermore, relatively little computational effort is required for frequencies at which the backshort performs well, so preliminary evaluations of potential designs can be accomplished very efficiently.

Also included in this paper are basic design guidelines for rectangular-hole backshorts. The hole widths are required to be at least 60% of the total waveguide width, and this will provide a good balance between mechanical strength and RF performance for submillimeter-wave applications. The length and spacing of the holes should have an electrical size between 65° and 105° at the center frequency, using the guided wavelength of the TE_{10} mode in the dielectric-filled gaps.

ACKNOWLEDGMENT

The authors would like to thank the reviewers for their scrutiny of this paper and their very helpful suggestions.

REFERENCES

[1] R. E. Collin, *Foundations for Microwave Engineering.* New York: McGraw-Hill, 1966, pp. 259–262.
[2] W. R. McGrath, "A novel non-contacting waveguide backshort for millimeter and submillimeter-wave frequencies," in *Proc. 2nd Nat. Technol. Transfer Conf.,* Dec. 1991, NASA Conf. Publ. 3136, vol. 1, pp. 161–168.
[3] W. R. McGrath, T. M. Weller, and L. P. Katehi, "A novel non-contacting waveguide backshort for submillimeter-wave frequencies," *Int. J. Infrared Millimeter Waves*, vol. 15, no. 12, 1994.
[4] W. R. McGrath, "Non-contacting waveguide backshort," U.S. Patent 5138289.
[5] T. Itoh, *Numerical Techniques for Microwave and Millimeter-Wave Passive Structures.* New York: Wiley, 1989.
[6] P. H. Masterman and P. J. B. Clarricoats, "Computer field-matching solution of waveguide transverse discontinuities," *Proc. IEE*, vol. 118, pp. 51–63, Jan. 1971.
[7] G. V. Eleftheriades, W. Y. Ali-Ahmad, P. B. Katehi, and G. M. Rebeiz, "Millimeter-wave integrated-horn antennas: Part I—Theory," *IEEE Trans. Antenn. Propagat.,* vol. 39, pp. 1575–1581, Nov. 1991.
[8] R. E. Collin, *Field Theory of Guided Waves.* Piscataway, NJ: IEEE Press, 1991, pp. 78–86.
[9] R. F. Harrington, *Field Computations by Moment Methods.* New York: Macmillan, 1968.
[10] N. I. Dib, P. B. Katehi, G. E. Ponchak, and R. N. Simons, "Theoretical and experimental characterization of coplanar waveguide discontinuities for filter applications," *IEEE Trans. Microwave Theory Tech.,* vol. 39, pp. 873–882, May 1991.
[11] N. I. Dib and P. B. Katehi, "Modeling of shielded CPW discontinuities using the space domain integral equation (SDIE)," *J. Electromagn. Waves Appl.,* vol. 5, no. 4/5, pp. 503–523, 1991.
[12] L. P. Dunleavy, "Discontinuity characterization in shielded microstrip: A theoretical and experimental study," Ph.D. dissertation, Radiation Lab., Univ. of Michigan, Ann Arbor, MI, 1988.
[13] N. Marcuvitz, *Waveguide Handbook*, vol. 10, MIT Rad. Lab. Series. New York: McGraw-Hill, 1948.
[14] A. Wexler, "Solution of waveguide discontinuities by modal analysis," *IEEE Trans. Microwave Theory Tech.,* vol. MTT-15, pp. 508–517, Sept. 1967.
[15] A. R. Kerr, "An adjustable short-circuit for millimeter waveguides," Electron. Div. Int. Rep. 280, National Radio Astronomy Observatory, Charlottesville, VA, July 1988.

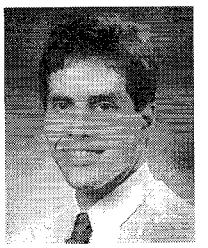

Thomas M. Weller (S'90) received the B.S.E.E. and M.S.E.E. degrees from the University of Michigan, Ann Arbor, in 1988 and 1991, respectively.

He is currently pursuing the Ph.D. degree in electrical engineering at the same university. His present research involves micromachining applications for microwave circuits and numerical modeling in electromagnetics.

Linda P. B. Katehi (S'81–M'84–SM'89) received the B.S.E.E. degree from the National Technical University of Athens, Greece, in 1977, and the M.S.E.E. and Ph.D. degrees from the University of California, Los Angeles, in 1981 and 1984 respectively.

In September 1984 she joined the faculty of the EECS Department of the University of Michigan, Ann Arbor. Since then, she has been involved in the development, modeling, fabrication, and experimental characterization of millimeter and near-millimeter-wave monolithic circuits and antennas.

Dr. Katehi was awarded the IEEE AP-S W. P. King Award in 1984, the IEEE AP-S S. A. Schelkunoff Award in 1985, the NSF Presidential Young Investigator Award, an URSI Young Scientist Fellowship in 1987, and the Humboldt Research Award in 1994. She is an Associate Editor for the IEEE Antennas and Propagation Society and of *Radio Science*. She is a member of Sigma XI, URSI Commission D, and an elected member of the IEEE Antennas and Propagation Society Administrative Committee.

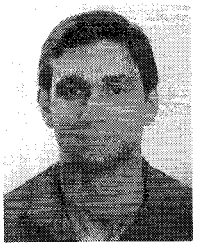

William R. McGrath (M'88) received the B.S. degree in physics from the Massachusetts Institute of Technology in 1978 and the M.A. and Ph.D. degrees in physics from the University of California, Berkeley, in 1981 and 1985, respectively. His graduate work focused on the device physics of SIS mixers and superconductive circuits. He and his co-workers were the first to measure the quantum effects of large gain and quantum-limited noise in SIS mixers at 36 GHz.

Upon graduation, he took a position as a visiting researcher at the Chalmers University of Technology, Goteborg, Sweden, where he worked on submillimeter-wave superconductive detectors. He and his co-workers there built the first millimeter-wave Josephson effect mixer using the newly discovered Hi-T_c superconductors. He joined the staff of the Jet Propulsion Laboratory in 1987, became a group leader in 1990, and a technical group supervisor in 1992. He heads a research group which develops high-performance submillimeter-wave sensors for remote-sensing applications. He has authored over 80 publications and holds two patents.

Dr. McGrath has received several awards related to his research activities.